

Protecting Quantum Information in Quantum Dot Spin Chains by Driving Exchange Interactions Periodically

John S. Van Dyke,¹ Yadav P. Kandel,² Haifeng Qiao,² John M. Nichol,² Sophia E. Economou,¹ and Edwin Barnes¹

¹*Department of Physics, Virginia Tech, Blacksburg, Virginia 24061, USA*

²*Department of Physics and Astronomy, University of Rochester, Rochester, NY, 14627 USA*

(Dated: September 21, 2020)

Recent work has demonstrated a new route to discrete time crystal physics in quantum spin chains by periodically driving nearest-neighbor exchange interactions in gate-defined quantum dot arrays [arXiv:2006.10913]. Here, we present a detailed analysis of exchange-driven Floquet physics in small arrays of GaAs quantum dots, including phase diagrams and additional diagnostics. We also show that emergent time-crystalline behavior can benefit the protection and manipulation of multi-spin states. For typical levels of nuclear spin noise in GaAs, the combination of driving and interactions protects spin-singlet states beyond what is possible in the absence of exchange interactions. We further show how to construct a time-crystal-inspired CZ gate between singlet-triplet qubits with high fidelity. These results show that periodically driving exchange couplings can enhance the performance of quantum dot spin systems for quantum information applications.

I. INTRODUCTION

Rapid theoretical and experimental development of quantum computers has led to a productive crossover of ideas between the fields of many-body condensed matter physics and of quantum information and computation^{1,2}. On the one hand, a principal application of quantum devices is the simulation of quantum many-body systems that are not amenable to classical computational methods³⁻⁵. However, the relationship is not merely one-way: concepts from many-body physics can also be useful in designing new quantum devices with improved information processing capabilities. This direction is exemplified by recent work on many-body localization, time crystals, and fractons⁶⁻¹¹, which have been variously proposed for robust storage of quantum information^{12,13}.

Studies of discrete time crystals (DTCs) in spin systems have largely employed single-spin rotations as the driving terms that are needed to realize the DTC phase^{6,7,14,15}. Such driving can be achieved in quantum dots (QDs), for instance, by electric dipole spin resonance (EDSR) via an embedded micromagnet¹⁶⁻¹⁹. But gate-defined QDs also afford exquisite control over spin interactions, whether by detuning or symmetric barrier gates²⁰⁻²². This motivates the exploration of novel driving protocols in which the spin interactions are periodically modulated. Driving the interactions also allows one to implement important operations, such as a SWAP between the states of neighboring QD spins, which is useful for measuring states in the middle of an array by shuttling the desired state to the edge for readout. A recent paper has developed a SWAP DTC driving protocol in which exchange driving of spin pairs by SWAP operations, followed by periods of weak interaction, produces time-crystal-like signatures in a four spin QD array²³.

In this paper, we explore the preservation and manipulation of entanglement in QD spin chains via the SWAP DTC protocol. We show that arbitrary states in the $S_z = 0$ subspace of two neighboring spins can be pre-

served for long times, with marked improvement over the undriven interacting system. This result, obtained for finite chains, is reminiscent of DTC physics in the thermodynamic limit, due to the crucial role played by interactions in stabilizing the state. It also suggests the application of the SWAP DTC protocol as a form of dynamic quantum memory, protecting the state of the two entangled spins. One may further consider such pairs of neighboring spins as forming singlet-triplet (ST) qubits^{20,24}. For this case, we design a universal gate set, which includes a high-fidelity CZ gate through the modification of the SWAP DTC protocol. Taken together, these results show that DTC-based physics offers a promising route for developing quantum information processing systems in solid-state spin arrays.

The paper is structured as follows. Section II introduces the model and the driving protocol for the SWAP DTC. Section III presents phase diagrams that demonstrate the robustness of the DTC phase to the presence of driving errors, a key requirement for the SWAP DTC to constitute a genuine phase of matter and to be of practical use. In Section IV, we investigate the time dependence of the return probability and uncover the existence of $4T$ periodic oscillations for initial entangled spin states, in contrast with the usual $2T$ time translation symmetry breaking found in earlier studies. Section V compares the return probabilities for different driving protocols and for the undriven Heisenberg spin chain, illustrating the importance of driving for preserving entangled states of the two spins in an ST qubit. Section VI demonstrates the single-qubit gate allowing for coherent switching of the preserved state. Section VII describes the CZ gate inspired by the SWAP DTC protocol and presents numerical calculations of its fidelity. Finally, the results are summarized in Section VIII.

II. MODEL OF A SWAP TIME CRYSTAL

We consider a one-dimensional chain of spin-1/2 degrees of freedom consisting of $L = 2N_q$ sites. The Hamiltonian for this system is given by

$$H = \sum_{\langle ij \rangle, \alpha} \frac{J_{ij}}{4} \sigma_i^\alpha \sigma_j^\alpha + \sum_i \frac{1}{2} (B_0 + \delta B_i) \sigma_i^z, \quad (1)$$

where $\alpha = \{x, y, z\}$ and $\langle ij \rangle$ indicates nearest-neighbors. J_{ij} is the exchange interaction, B_0 is an externally applied uniform magnetic field, and δB_i is a random Gaussian-distributed contribution to the total field with variance σ_B due to nuclear spin noise (as in GaAs, for instance).

Although the principles we discuss apply to generic spin-1/2 Heisenberg chains, we find it helpful to think of the system as an array of coupled ST qubits²⁴. An ST qubit consists of a pair of electron spins on neighboring QDs subject to a large magnetic field that separates out the polarized states, $|T_+\rangle = |\uparrow\uparrow\rangle$ and $|T_-\rangle = |\downarrow\downarrow\rangle$, leaving behind the computational subspace $\{|S\rangle, |T_0\rangle\}$ of the singlet ($|S\rangle = (|\uparrow\downarrow\rangle - |\downarrow\uparrow\rangle)/\sqrt{2}$) and $S_z = 0$ triplet ($|T_0\rangle = (|\uparrow\downarrow\rangle + |\downarrow\uparrow\rangle)/\sqrt{2}$) states. The resulting two-level system admits a Bloch sphere representation, as shown in Fig. 1, where the basis $\{|\uparrow\downarrow\rangle, |\downarrow\uparrow\rangle\}$ is chosen for the \hat{z} direction. ST qubits are actively being studied as an encoding for qubits that are naturally insensitive to uniform magnetic field fluctuations^{20,25-31}. N_q is the number of ST qubits in the chain, which are comprised of pairs of neighboring sites $(2q-1, 2q)$, with $q = 1, 2, \dots$ (Fig. 1).

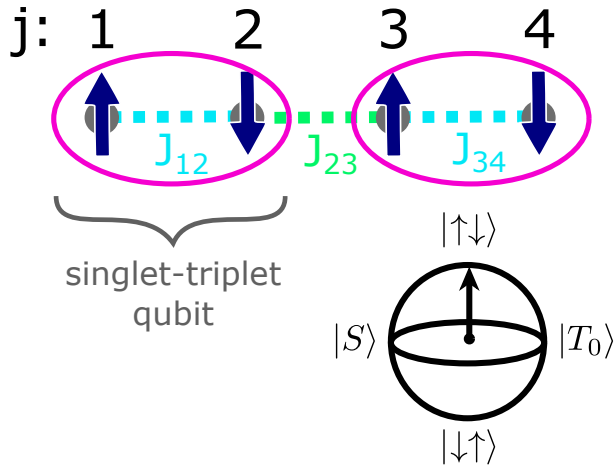


FIG. 1. Schematic of an $L = 4$ Heisenberg spin chain with variable exchange interactions J_{12} , J_{23} , and J_{34} . One can think of this system as a pair of coupled ST qubits (with leakage), as indicated by the purple ovals. J_{12} and J_{34} are used to execute SWAP operations on the spins defining these qubits, while J_{23} yields an interaction between them. The ST qubit Bloch sphere is also shown.

Time crystalline phases were previously discovered in driven Heisenberg chains by applying tailored “H2I”

pulse sequences or magnetic field gradients that convert the Heisenberg interactions into effective Ising ones^{32,33}. In both approaches, the periodic driving consisted of single-particle terms that rotate the spins by π , whether by idealized δ -function pulses or realistic EDSR methods. Notably, it was found to be necessary to apply H2I pulses or field gradients in order to stabilize a DTC for the levels of magnetic field noise present in experiment (e.g. 18 MHz in GaAs, such that $T_2^* \approx 10$ ns).

Here, we consider a driving protocol based on varying the exchange interactions in a QD array, instead of single-spin manipulations. This approach has several advantages. For one, it can be performed in systems that lack the micromagnet needed for EDSR. More importantly, the timescales for modifying the nearest-neighbor exchange are very fast (a few nanoseconds), whereas EDSR is slower for the weak to moderate field gradients typically used in experiment¹⁶. The fundamental idea of our approach is to drive the system periodically by fast SWAP operations within each ST qubit, followed by long evolution times during which neighboring ST qubits interact²³. Both of these operations are implemented by the same underlying physical mechanism, namely, the nearest-neighbor exchange coupling between QD spins. More specifically, we consider the following unitary evolution over one drive period:

$$U = U_{SWAP}(T_S) U_{evo}(T_e). \quad (2)$$

The two parts of this protocol are piecewise constant, with the SWAP piece given by $U_{SWAP}(T_S) = e^{-iH_S T_S}$, where

$$H_S = \frac{J_S}{4} (1 - \epsilon) \sum_{i=1, \alpha}^{L/2} \sigma_{2i-1}^\alpha \sigma_{2i}^\alpha + \sum_{i=1}^L \frac{1}{2} (B_0 + \delta B_i) \sigma_i^z \quad (3)$$

is applied for time T_S such that $J_S T_S = \pi$, thus interchanging the spin states of sites $2i-1$ and $2i$. ϵ introduces a fractional error in the SWAP pulse, corresponding to an underrotation for $\epsilon > 0$. For the $L = 4$ chain, the SWAP interactions are illustrated by the light blue dashed lines in Fig. 1, such that $J_{12} = J_{34} = J_S$. The evolution piece $U_{evo}(T_e) = e^{-iH_e T_e}$ is generated by the Hamiltonian

$$H_e = \frac{J_e}{4} \sum_{i=1, \alpha}^{L/2-1} \sigma_{2i}^\alpha \sigma_{2i+1}^\alpha + \sum_{i=1}^L \frac{1}{2} (B_0 + \delta B_i) \sigma_i^z. \quad (4)$$

These interactions are indicated by the light green dashed line in Fig. 1, with $J_{23} = J_e$. In the following sections, we explore the consequences of this driving protocol for the stabilization of quantum information. Unless otherwise stated, we assume an $L = 4$ chain in our numerical calculations. The calculations were performed using the QuSpin Python package for exact diagonalization of quantum many-body systems³⁴.

III. PHASE DIAGRAMS

One of the defining features of a time crystal is its stability to perturbations due to the presence of non-zero interactions in the system. Earlier work on both Ising model and Heisenberg model DTCs has shown that sufficiently weak driving pulse errors (i.e. over- or under-rotation of the spins relative to π radians) do not destroy the phase. Here we examine the corresponding errors in performing an incomplete SWAP operation. Fig. 2(a) shows the subsystem return probability for qubit 1 (sites 1 and 2) of an $L = 4$ spin chain, after four periods of the protocol ($n_T = 4$). The system is initialized in the product state in which each ST qubit is in its individual non-interacting ground state, the latter being determined by the local magnetic field gradient across the double QD. Thus, the initial state chosen varies over the field noise disorder realizations. This scenario is naturally realized in experiments with gate-defined QD arrays. In our calculations, we fix the evolution time to $T_e = 1.4 \mu\text{s}$, and we vary the interaction strength J_e and the fractional error in performing a SWAP, i.e. an error of $\epsilon = 0.5$ corresponds to a $\sqrt{\text{SWAP}}$, while for $\epsilon = 1$ no operation is performed at all. We find that typical levels of charge noise have little effect on the results, so we neglect this here. The wedge-shaped regions of high return probability for small ϵ and increasing J_e illustrate that interactions are crucial for preserving the quantum state of qubit 1 in the presence of driving errors. We note that not driving the system at all ($\epsilon = 1$) is also very effective for preserving the state of qubit 1 (though of course in this case there is no time translation symmetry breaking). We examine this further in Section V.

In contrast, Fig. 2(b) reveals that when qubit 1 is initialized in a singlet state, SWAP driving is required to produce a high return probability after four periods of evolution. Here, the initial state of qubit 2 is still the product state determined by the local field gradient. While $J_e = 0$ yields a high singlet return probability for a perfect SWAP, the presence of finite interactions does increase the value of the return probability, as seen in Fig. 3. The singlet return probability peaks when $J_e T_e = \pi n$ (for J_e measured in $\text{rad}/\mu\text{s}$). In weak magnetic field gradients, these values correspond to performing n SWAP operations on sites belonging to different neighboring qubits (e.g. sites 2 and 3 in the $L = 4$ chain). An even n yields a net trivial operation (for perfect SWAPs), while odd n causes the initial singlet on sites 1 and 2, S_{12} , to be transferred to sites 1 and 3 during the evolution piece of the protocol, which is then undone after three additional periods in the $L = 4$ case. The low values of S_{12} in between the peaks can be understood as arising from the monogamy of entanglement, since an incomplete SWAP leads to site 1 remaining partially entangled with the rest of the chain after four periods, and thus less entangled with site 2. When the initial state is the product state $|\uparrow\downarrow\rangle|\uparrow\downarrow\rangle$, the SWAP on 2 and 3 produces a spin echo-like effect that accounts for the maxima when n is odd.

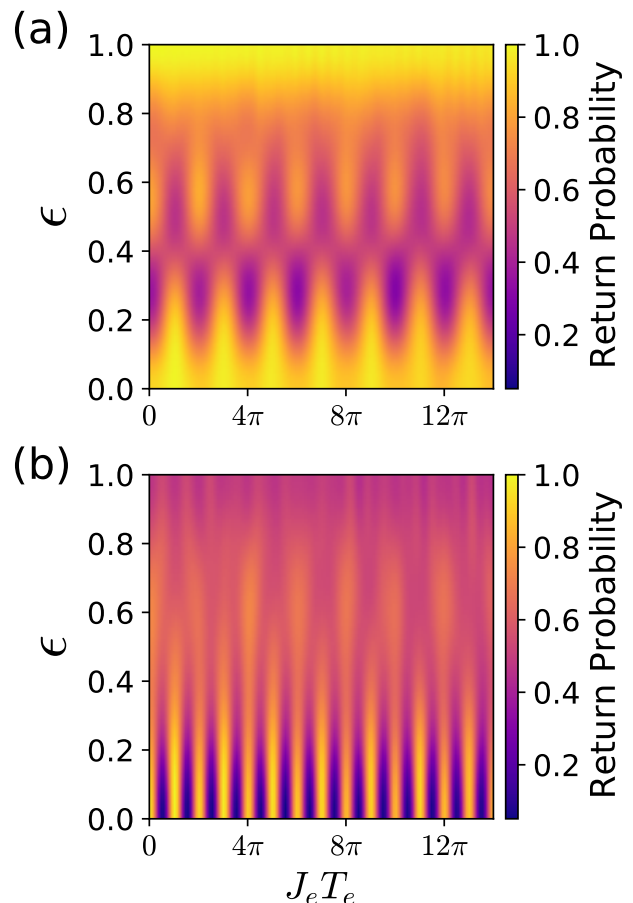


FIG. 2. (a) Phase diagram of the return probability for an initial $|\uparrow\downarrow\rangle$ state on qubit 1 as a function of inter-qubit coupling J_e and pulse error ϵ . (b) Phase diagram of the return probability for an initial singlet state of qubit 1. Parameters are $L = 4$, $B_0 = 3075$ MHz, $\sigma_B = 18$ MHz, $T_e = 1.4 \mu\text{s}$, $T_S = 2$ ns, $J_S = \pi/T_S$, $n_T=4$. Here we have chosen parameters similar to those of Ref.²³. The initial state of qubit 2 is the product state that minimizes the field gradient energy for a given disorder realization. Results are averaged over 192 disorder realizations.

IV. RETURN PROBABILITY DYNAMICS

The dynamics are also different depending on whether the initial state is a product or singlet state. Fig. 4 illustrates the $2T$ periodicity of the return probability for qubit 1 when the system is initialized in $|\uparrow\downarrow\rangle|\uparrow\downarrow\rangle$ and $J_e T_e = \pi$. The results agree with those for a chain driven by single-spin π rotations, as both operations have the same effect: $|\uparrow\downarrow\rangle|\uparrow\downarrow\rangle \rightarrow |\downarrow\uparrow\rangle|\downarrow\uparrow\rangle$.

On the other hand, the $L = 4$ chain shows a $4T$ periodicity for the singlet return probability of qubit 1. This is in striking contrast with previous work on discrete time crystals, which generally found a $2T$ periodicity for spin-1/2 degrees of freedom^{6,7,14,15}. In fact, for $\sigma_B \ll J_e$ we find that an L site chain has a singlet return probability with LT periodicity. This can be easily understood

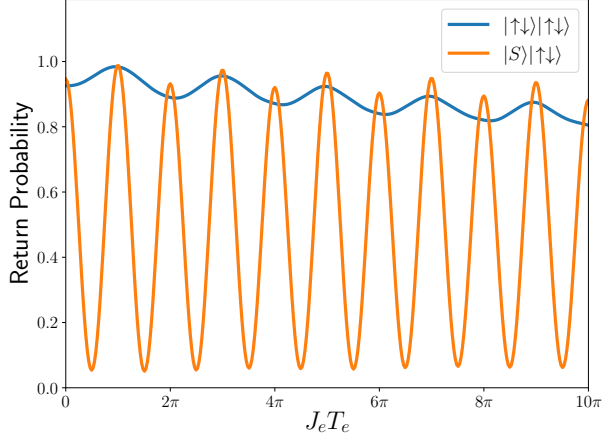


FIG. 3. Return probability for qubit 1 as a function of $J_e T_e$, for the initial states $|\uparrow\downarrow\rangle$ (blue line) and the singlet (orange line). Parameters are $L = 4$, $B_0 = 3075$ MHz, $\sigma_B = 18$ MHz, $J_S = 250$ MHz, $T_e = 1.4$ μ s, $T_S = 2$ ns, $n_T=4$, $\epsilon = 0$. The initial state of qubit 2 is $|\uparrow\downarrow\rangle$. Results are averaged over 960 disorder realizations.

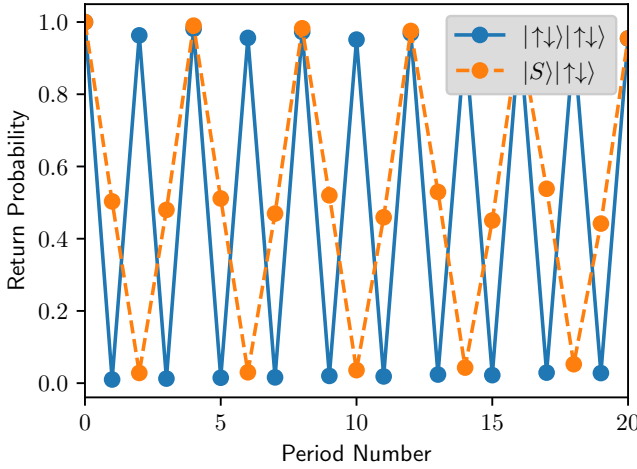


FIG. 4. Time dependence of the return probabilities for qubit 1, given an initial state of $|\uparrow\downarrow\rangle$ for qubit 2. The blue line shows the return probability for $|\uparrow\downarrow\rangle$, given the initial product state $|\uparrow\downarrow\rangle|\uparrow\downarrow\rangle$. The orange shows the return probability for the singlet state $|S\rangle$, given the initial product state $|S\rangle|\uparrow\downarrow\rangle$ (orange line). Parameters are $L = 4$, $B_0 = 3075$ MHz, $\sigma_B = 18$ MHz, $T_e = 1.4$ μ s, $J_e = \pi/T_e$, $T_S = 2$ ns, $J_S = \pi/T_S$, $\epsilon = 0$. Results are averaged over 6000 disorder realizations.

as arising from successive applications of SWAPs, coming from both the explicit driving part of the protocol and the evolution part tuned to $J_e T_e = \pi$. For instance, when $L = 6$ we have the following steps that transfer the singlet state down the chain, where it is “reflected” off the

right edge and returns back to its initial position:

$$\begin{aligned} S_{12} &\xrightarrow{\text{SWAP}} S_{12} \xrightarrow{\text{evo}} S_{13} \xrightarrow{\text{SWAP}} S_{24} \xrightarrow{\text{evo}} S_{35} \\ &\xrightarrow{\text{SWAP}} S_{46} \xrightarrow{\text{evo}} S_{56} \xrightarrow{\text{SWAP}} S_{56} \xrightarrow{\text{evo}} S_{46} \\ &\xrightarrow{\text{SWAP}} S_{35} \xrightarrow{\text{evo}} S_{24} \xrightarrow{\text{SWAP}} S_{13} \xrightarrow{\text{evo}} S_{12} \end{aligned} \quad (5)$$

However, the experimentally relevant interaction strength needed to perform a single SWAP over 1.4 μ s is ~ 350 kHz, which is much smaller than the magnetic field noise ~ 18 MHz in GaAs QDs. For realistic levels of field noise, the singlet return probability displays a $4T$ periodicity regardless of chain length. Moreover, we find that when the disorder starts at small values and increases toward 18 MHz, the transition between $6T$ and $4T$ periodicity is smooth, with the return probability at $6T$ gradually decreasing while that at $4T$ increases (as opposed to a shift in the peak from $6T$ to $4T$ through intermediate values).

The $4T$ periodicity observed at sufficiently strong disorder can be explained as follows. First, note that each part of the protocol involves interactions only between disjoint pairs of spins. Thus, we may consider the Hamiltonian, Eq. (1), restricted to two sites a and b ,

$$H_{ab} = \frac{J}{4}(\sigma_a^x \sigma_b^x + \sigma_a^y \sigma_b^y + \sigma_a^z \sigma_b^z) + \frac{1}{2}(B_a \sigma_a^z + B_b \sigma_b^z), \quad (6)$$

where $B_{a,b}$ is the total field at site a, b . In general, the two spins coupled in a given part of the protocol can have parallel or antiparallel orientations. Within the $\{|\uparrow\downarrow\rangle, |\downarrow\uparrow\rangle\}$ subspace the evolution operator $U = e^{-itH_{ab}}$ is

$$U_1 = e^{iJt/2} \begin{pmatrix} \cos(\frac{\alpha t}{2}) + \frac{i\Delta}{\alpha} \sin(\frac{\alpha t}{2}) & -\frac{iJ}{\alpha} \sin(\frac{\alpha t}{2}) \\ -\frac{iJ}{\alpha} \sin(\frac{\alpha t}{2}) & \cos(\frac{\alpha t}{2}) - \frac{i\Delta}{\alpha} \sin(\frac{\alpha t}{2}) \end{pmatrix}, \quad (7)$$

with $\alpha = \sqrt{J^2 + \Delta^2}$ and $\Delta = B_b - B_a$ the field gradient across the pair. We have multiplied U (and hence U_1) by a global phase, $e^{iJt/4}$, to simplify the following analysis. The SWAP part of the protocol is performed in 2 ns, so that $J_S \gg \Delta$ and we may neglect errors in the transition $|\uparrow\downarrow\rangle \xrightarrow{\text{SWAP}} |\downarrow\uparrow\rangle$. For the evolution part of the protocol we use perturbation theory in (J_e/Δ) to obtain the approximate evolution

$$U_1' = e^{iJ_e t/2} \begin{pmatrix} e^{i\Delta t/2} & 0 \\ 0 & e^{-i\Delta t/2} \end{pmatrix}. \quad (8)$$

On the other hand, the evolution in the $\{|\uparrow\uparrow\rangle, |\downarrow\downarrow\rangle\}$ subspace is given by

$$U_2 = \begin{pmatrix} e^{-iB_{tot}t/2} & 0 \\ 0 & e^{iB_{tot}t/2} \end{pmatrix}, \quad (9)$$

where $B_{tot} = B_a + B_b$. Now starting from the initial state $|\psi_0\rangle = (|\uparrow\downarrow\rangle - |\downarrow\uparrow\rangle)|\uparrow\downarrow \dots\rangle$ (suppressing the normalization of the state) and successively applying SWAPs

and the evolutions in Eq. (8) and Eq. (9), we find

$$|\psi_0\rangle \rightarrow |\psi_1\rangle = ie^{i\Delta T_e/2}|\downarrow\uparrow\downarrow\uparrow\dots\rangle - e^{iB_{tot}T_e/2}|\uparrow\downarrow\downarrow\uparrow\dots\rangle \quad (10)$$

after the first period, where we used that $e^{iJ_e T_e/2} = i$, and we ignored accumulated phases coming from spins other than the first three. The second period of the protocol yields

$$|\psi_1\rangle \rightarrow |\psi_2\rangle = -(|\uparrow\downarrow\rangle + |\downarrow\uparrow\rangle)|\uparrow\downarrow\dots\rangle, \quad (11)$$

so that the first qubit is in the state $|T_0\rangle$. Two further periods then recover the initial state on sites 1 and 2, explaining the $4T$ periodicity of the singlet return probability.

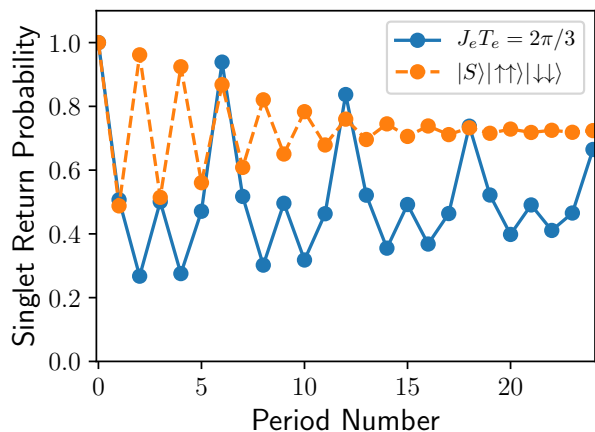


FIG. 5. Singlet return probability for the cases in which the total phase accumulation of the evolution part of the protocol is $J_e T_e = 2\pi/3$ (blue line) and in which the initial state is $|S\rangle|\uparrow\uparrow\rangle|\downarrow\downarrow\rangle$ (orange line). In the first case, the initial state is the singlet state for qubit 1 and the product states minimizing the field gradient energies for the other qubits. In the second case, $J_e T_e = \pi$. Other parameters are $L = 6$, $B_0 = 3075$ MHz, $\sigma_B = 18$ MHz, $T_e = 1.4 \mu\text{s}$, $T_S = 2$ ns, $J_S = \pi/T_S$, $\epsilon = 0$. Results are averaged over 6000 disorder realizations.

To provide further support for this simple physical picture, we consider two extensions of the idea. We note the $4T$ periodicity fundamentally arises from the phase factor $e^{iJ_e t/2}$ in Eq. (8) becoming trivial after four periods, when $J_e T_e = \pi$ (here J is given in radians and $\hbar = 1$). Thus, one should obtain a different periodicity when $J_e T_e$ is chosen such that the relative phase winding occurs at another rate. That this is indeed the case is shown in Fig. 5, where $J_e T_e = 2\pi/3$ and the resulting periodicity of the singlet return probability maxima is $6T$. Alternatively, one may consider initializing the second qubit in the state $|\uparrow\uparrow\rangle$ (with the first qubit still initialized in $|S\rangle$). A similar argument as above shows that the first qubit returns to the singlet state after $2T$, in agreement with the orange curve in Fig. 5. In longer chains, a singlet state prepared in the bulk experiences

$4T$ periodicity of the return probability at an interaction strength $J_e T_e = \pi/2$, half the value for a ST qubit on the edge. This is essentially due to the increased number of neighbors, and mirrors the case of the single spin return probability, for which the phase diagram of a bulk spin has half the period compared to that for an edge spin³³.

V. COMPARISON WITH THE UNDRIVEN SYSTEM

As noted in Section III, the product state $|\uparrow\downarrow\rangle$ on qubit 1 is well-preserved even in the absence of SWAP driving. In Fig. 6(a) we study the return probability as a function of time, for several different driving protocols. Two different undriven cases are presented. In the first, the Heisenberg interactions are equal throughout the chain and set to the same value as used for the SWAP driving evolution: $J_{12} = J_{23} = J_{34} = \pi/T_e$. However, since the SWAP DTC evolution piece only involves inter-qubit J_e , the second undriven case mirrors this by setting $J_{23} = \pi/T_e$ and $J_{12} = J_{34} = 0$. In either case, while the undriven and SWAP-driven cases perform similarly up to ten periods, in the long-time limit the undriven cases are clearly superior. The saturation value of the return probability for the undriven cases tends to grow with increasing field noise strength³⁵. We note, however, that it does not ultimately approach 1 in the large noise limit. This is due to the fact that disorder averaging mixes in unfavorable field configurations, which limits the overall return probability. On the other hand, applying a uniform linear field gradient (not shown) does tend to increase the return probability towards 1, as the gradient strength increases.

We also compare the SWAP protocol to more traditional single-spin driving. Thus, we consider an idealized instantaneous π rotation of all the spins (i.e. a delta-pulse in time):

$$V_\delta(t) = \frac{\pi}{2} \sum_{s=1}^{\infty} \delta(t - sT) \sum_{j=1}^L \sigma_j^x. \quad (12)$$

In this case, all nearest-neighbor exchange interactions are turned on, as in the first undriven case. The period of the delta-pulses is adjusted to coincide with the total period of SWAP driving cases, $T_\delta = T_e + T_S$. Fig. 6(a) shows that for an initial product state, the SWAP driving is preferable to the single-spin rotations of the delta-pulse case for experimentally relevant levels of magnetic field noise.

Turning to the case where qubit 1 is initially in an entangled state, it is apparent from Fig. 6(b) that an initial singlet state is not at all preserved for the undriven protocols, whereas the SWAP case leads to a high return probability every four periods, in accordance with the results above. In the given parameter regime, we again see that delta-pulse single-spin rotations are inferior to SWAP pulses for preserving the initial state.

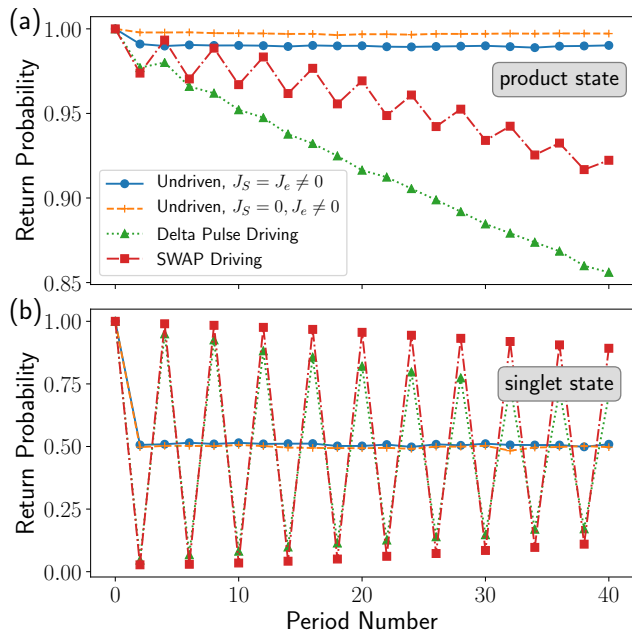


FIG. 6. (a) Comparison between the undriven system and driving protocols, for an initial product state that minimizes the field gradient energy of qubit 1. (b) Comparison between the undriven system and driving protocols, for an initial singlet state of qubit 1. Other parameters are $L = 4$, $B_0 = 3075$ MHz, $\sigma_B = 18$ MHz, $T_e = 1.4 \mu\text{s}$, $J_e = \pi/T_e$. For the SWAP driving case $T_S = 2$ ns, $J_S = \pi/T_S$, and for both driven cases $\epsilon = 0$. The initial state of qubit 2 is the one minimizing the field gradient energy. Results are plotted stroboscopically for every $2T$ and averaged over 6000 disorder realizations.

We have seen that the product states $|\uparrow\downarrow\rangle$ and $|\downarrow\uparrow\rangle$ survive longer in the absence of SWAP driving, whereas $|S\rangle$ and $|T_0\rangle$ are preserved better when the system is driven. This suggests that if we consider “unbalanced” superpositions $\cos(\theta/2)|\uparrow\downarrow\rangle - \sin(\theta/2)|\downarrow\uparrow\rangle$ where $0 < \theta < \pi/2$, there should exist some value θ_* such that for $\theta > \theta_*$, driving is beneficial for state preservation. The value of θ_* in fact depends on how long one wishes to preserve the state, as is shown in Fig. 7. The undriven system return probabilities depend strongly on θ , but are essentially time-independent after an initial decay. Here we have considered the first type of undriven system, in which all nearest-neighbor exchange interactions are nonzero and equal. In contrast, SWAP driving leads to a steady decay of the return probability as the number of driving periods is increased; this decay is relatively insensitive to θ . The intersection of the return probability curves for the undriven and SWAP-driven cases yields the time below which SWAP driving enhances the attainable return probability for a given initial state parameterized by θ . Conversely, we may fix the time scale at a desired value and then read off the value of θ_* by adjusting θ until the undriven return probability curve intersects the SWAP-driving curve at that time. Similar results are obtained for states with complex coefficients (not shown). Aver-

aging over 88 states approximately distributed equally across the Bloch sphere, the undriven system yields a return probability of 0.65 after 40 periods, compared to 0.90 for the SWAP driven case. This indicates that a generic state is much better preserved by driving the system with the SWAP DTC protocol.

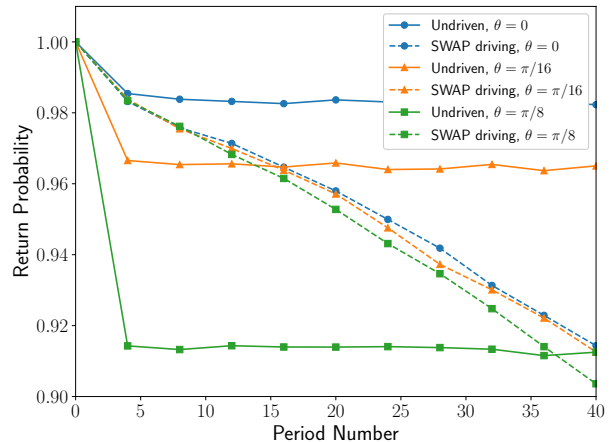


FIG. 7. Comparison between the undriven (first case; all nearest neighbor interactions on) (solid lines) and SWAP-driven (dashed lines) systems when qubit 1 is initialized in $\cos(\theta/2)|\uparrow\downarrow\rangle - \sin(\theta/2)|\downarrow\uparrow\rangle$. Results are shown for $\theta = 0, \pi/16, \pi/8$. Results are plotted stroboscopically every $4T$. Other parameters are $L = 4$, $B_0 = 3075$ MHz, $\sigma_B = 18$ MHz, $T_e = 1.4 \mu\text{s}$, $J_e = \pi/T_e$. For the driven case, $T_S = 2$ ns, $J_S = \pi/T_S$, $\epsilon = 0$. The initial state of qubit 2 is $|\uparrow\downarrow\rangle$. Results are averaged over 6000 disorder realizations.

VI. SWITCHING PRESERVED STATES

In the course of an information processing task, it is necessary to be able to change what state is stored in the memory. In Fig. 8(a) we show that an initial $|S\rangle$ state, preserved for 20 periods, can be switched to the $|T_0\rangle$, and subsequently preserved to a similar degree. The switching operation is performed simply by inserting an additional two periods with $J_e = 0$, halfway through the experimental run.

More generally, one can switch from $|S\rangle$ to an arbitrary state of the form $|\uparrow\downarrow\rangle + e^{i\alpha}|\downarrow\uparrow\rangle$ by adjusting the value of J_e during the two extra periods, such that $J_e T_e = \alpha$. Fig. 8(b) shows that the return probability for the new state after ~ 40 total periods of evolution remains large, regardless of the choice of α .

VII. IMPLEMENTING TWO-QUBIT GATES

While the preservation of quantum states is an important task for quantum computing, it is also necessary to manipulate states and execute various logical gates.

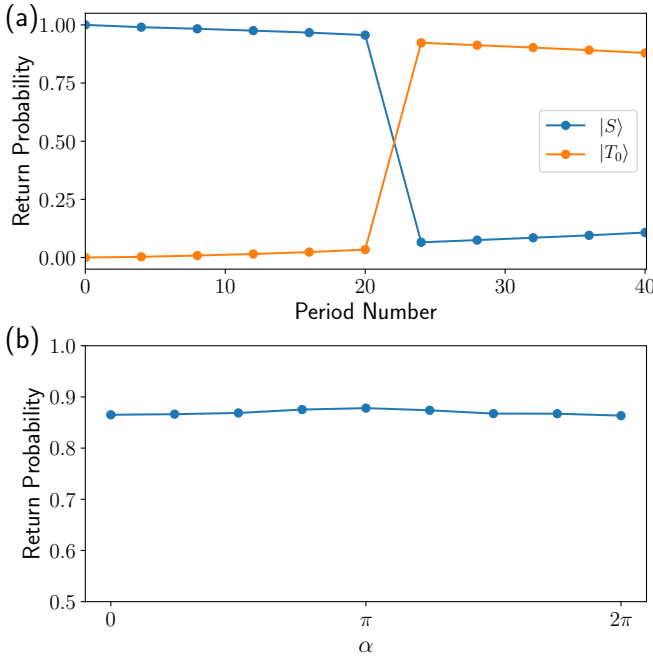


FIG. 8. (a) Return probabilities for qubit 1 for the singlet (blue line) and triplet (orange line) states, for a system initialized in the singlet state for qubit 1 and subject to the switching protocol half way through the total evolution. (b) End time return probability for the state $|\psi\rangle = |\uparrow\downarrow\rangle + e^{-i\alpha}|\downarrow\uparrow\rangle$ for qubit 1, when it is initialized in the singlet state and subject to the switching protocol half way through the evolution. Other parameters are $L = 4$, $B_0 = 3075$ MHz, $\sigma_B = 18$ MHz, $T_e = 1.4 \mu\text{s}$, $J_e = \pi/T_e$. The initial state of qubit 2 is $|\uparrow\downarrow\rangle$. Results are averaged over 6000 disorder realizations.

Here we explore the possibility of using the SWAP driving protocol to realize two-qubit gates in a chain of ST qubits. We first note that when qubit 1 is initialized in a singlet state, the return probability oscillates with period $4T$ ($2T$) if qubit 2 is in state $|\uparrow\downarrow\rangle$ ($|\uparrow\uparrow\rangle$). This implies that the evolution after two periods is equivalent (up to single-qubit rotations) to a CNOT gate, where qubit 1 is the target, and qubit 2 is the control, since qubit 1 flips from $|S\rangle$ to $|T_0\rangle$ depending on whether the spins in qubit 2 are parallel or antiparallel. However, this approach suffers from the disadvantage that parallel spin states are not part of the computational subspace of ST qubits. Conditional control of individual spins using ESR or EDSR would alleviate this issue by allowing one to temporarily map $|\downarrow\uparrow\rangle \rightarrow |\downarrow\downarrow\rangle$ to execute the CNOT, before restoring the $|\downarrow\uparrow\rangle$ state of the control bit.

Another approach is based on the effective Ising Hamiltonian between exchange-coupled ST qubits in a linear array³⁶. An Ising interaction of the appropriate duration can be converted to a CZ gate by applying additional single-qubit rotations³⁷:

$$CZ = e^{-i\pi/4} e^{i\pi\sigma_1^z/4} e^{i\pi\sigma_2^z/4} e^{-i\pi\sigma_1^z\sigma_2^z/4} \quad (13)$$

This suggests viewing the protocol for the SWAP time

crystal not only as a means of state preservation, but also as a way to generate two-qubit gates. Indeed, whereas two periods of the protocol U of Eq. (2) yield the best state preservation when $J_e T_e = \pi$ (for product states of a single qubit), setting $J_e T_e = \pi/2$ produces a CZ gate when followed by single-qubit rotations on each ST qubit, due to the effective Ising interaction between the ST qubits. Later, we compare this two-period gate to one that uses a single period of SWAP DTC evolution. We numerically study the CZ protocol in the $L = 4$ spin chain, configured as two ST qubits. The accuracy of the proposed gate can be assessed by looking at the probability of finding the evolved spins in the state that would be obtained from an ideal CZ gate: $p_{CZ} = |\langle CZ_{ideal,i} | CZ_{actual,i} \rangle|^2$. Here, $|CZ_{actual,i}\rangle = U_{CZ}|\psi_i\rangle$ and $|CZ_{ideal,i}\rangle = CZ|\psi_i\rangle$, where truncation of the state to the logical subspace is implicit. The physically implemented gate is given by

$$U_{CZ} = \mathcal{R}_{z,\pi/2}^{(1,2)} [U_{SWAP}(T_S) U_{evo}(T_e)]^2, \quad (14)$$

where the exchange coupling J_e in U_{evo} is such that $J_e T_e = \pi/2$, while J_S in $U_{SWAP}(T_S)$ remains the value required for a SWAP operation: $J_S T_S = \pi$. The operation $\mathcal{R}_{z,\pi/2}^{(1,2)}$ implements a simultaneous rotation on each qubit by $\pi/2$.

The fact that U_{CZ} approximates a CZ gate can be seen by noticing that in the physically relevant parameter regime where $J_S \gg \Delta$ and $J_e \ll \Delta$, where Δ is the magnetic field gradient across neighboring QDs, the evolution (truncated to the logical subspace) after two periods is approximately given by

$$[U_{SWAP}(T_S) U_{evo}(T_e)]^2 \approx \begin{pmatrix} i & 0 & 0 & 0 \\ 0 & 1 & 0 & 0 \\ 0 & 0 & 1 & 0 \\ 0 & 0 & 0 & i \end{pmatrix} \quad (15)$$

in the basis $\{|0\rangle|0\rangle, |0\rangle|1\rangle, |1\rangle|0\rangle, |1\rangle|1\rangle\}$, with $|0\rangle = |\uparrow\downarrow\rangle$ and $|1\rangle = |\downarrow\uparrow\rangle$ forming the logical basis of the ST qubits. This result can be obtained using the approximate expressions for each piece of the evolution given in Sec. IV. The subsequent application of the z rotations on each ST qubit as indicated in Eq. (14) converts the right-hand side of Eq. (15) into a CZ gate. Below, we show that the discrepancy between U_{CZ} and CZ is mostly due to additional single-qubit gates that arise from terms of order Δ/J_S and J_e/Δ . Thus, U_{CZ} remains locally equivalent to a CZ gate even when these higher-order effects are included.

In Fig. 9(a) we present numerical results for the CZ gate probability, p_{CZ} , for 100 randomly selected initial product states of the ST qubits: $|\psi_i\rangle = |\psi_i^{(1)}\rangle |\psi_i^{(2)}\rangle$. Despite the single-qubit gates caused by finite Δ/J_S and J_e/Δ , the mean probability is high: $\bar{p}_{CZ} = 0.991$. The use of more complicated pulse shaping techniques that effectively remove these extra local gates can be expected to improve this result further^{26,38,39}. Unless noted otherwise, calculations are performed with fixed field gradients across

	G_1	G_2	G_3
Actual CZ	3.5×10^{-5}	-4.1×10^{-7}	$1 + 3.9 \times 10^{-5} - 9.0 \times 10^{-7}i$
Ideal CZ	0	0	1

TABLE I. Makhlin invariants for the SWAP-DTC two-qubit CZ gate. Parameters are the same as in Fig. 9.

each ST qubit, without any “noise” component. Corrective pulse shaping can be designed using the knowledge of these gradients to produce a pure CZ gate. In our simulations, the $\mathcal{R}_{z,\pi/2}^{(1,2)}$ operation is implemented by allowing each ST qubit to precess freely under its respective field gradients for a time $(T_g - t_r - 2T_S)/2$. Here $T_g = 1 \mu\text{s}$ is the total gate time, while

$$t_r = \begin{cases} \pi/(2\Delta) & \text{if } \Delta > 0 \\ 3\pi/(2\Delta) & \text{if } \Delta < 0 \end{cases} \quad (16)$$

After this precession, a SWAP pulse is applied and the qubit is allowed to precess again until $T_g - T_S$, at which time a final SWAP is applied. This process allows for the rotation of the single-qubit state, along with an additional spin-echo-like part that keeps the different qubits in sync. Below, we also consider the noisy situation in which the true values of the gradients deviate from the ones assumed by the experimentalist implementing the gate.

To assess the intrinsic entangling properties of the physical two-qubit CZ, we compute the Makhlin invariants G_1 , G_2 , and G_3 , which characterize a given two-qubit gate up to arbitrary single-qubit rotations^{40,41}. The Makhlin invariants for an ideal CZ are $G_1 = G_2 = 0$ and $G_3 = 1$. Fig. 9(b) shows the Makhlin invariants for the physical CZ as functions of the inter-qubit coupling J_e . For the optimal value $J_e = \pi/(2T_e)$, the values of $G_{1,2,3}$ are given in Table I. One sees that the invariants of the physical gate closely approximate those of the ideal one. This suggests that errors in the single-qubit rotations are the main factor leading to the imperfect CZ probabilities shown in Fig. 9(a). We also note that G_3 is necessarily real for any two-qubit gate. Thus, the small imaginary part in the numerical calculation must arise due to leakage out of the computational subspace. Fig. 9(b) indicates that significant departures from the optimal J_e lead to non-negligible errors in G_1 and G_3 . Thus, precise experimental control over the magnitude of J_e is important for realizing the desired gate. For a value of J_e that is 1% larger than optimal one, however, G_3 remains well within 0.01% of its ideal value.

One should also consider variations in the magnetic field gradients across the two qubits. While these can be controlled to some extent, for instance, by micromagnet design, there are also contributions due to nuclear spin noise. Fig. 10 shows the Makhlin invariants for the physical CZ gate as functions of the magnetic field gradients across qubits 1 and 2, respectively (the left spins of each

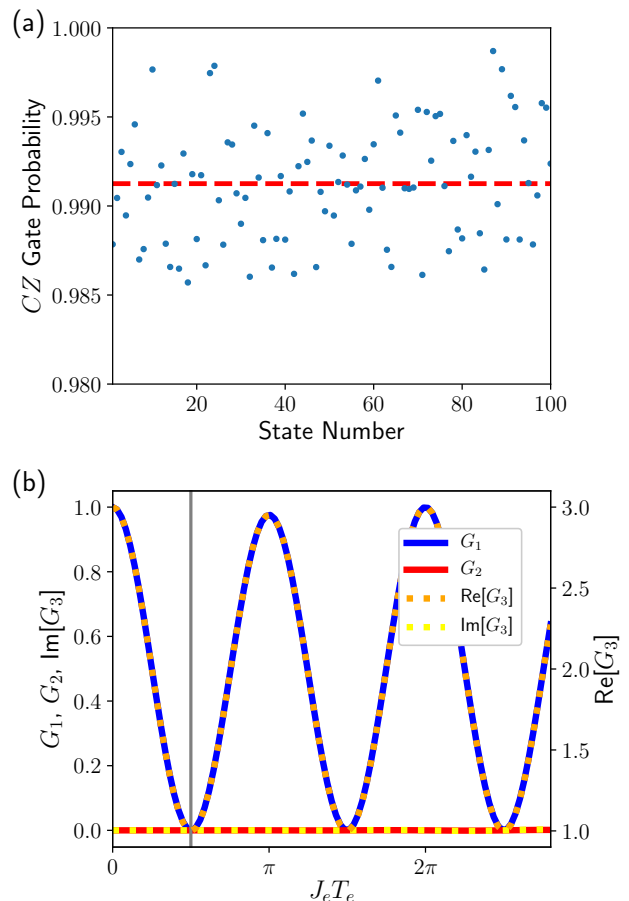


FIG. 9. (a) Probability $p_{\text{CZ}} = |\langle \text{CZ}_{\text{ideal}} | \text{CZ}_{\text{actual}} \rangle|^2$ of finding the spin chain in the state that would be produced by an ideal CZ gate after the sequence in Eq. (14) is applied. $J_e = \pi/(2T_e)$, with $T_e = 1.4 \mu\text{s}$, as indicated by the vertical gray line in panel (b). Initial states are random product states in the ST qubit logical subspace. The red dashed line indicates the mean CZ gate probability $\overline{p_{\text{CZ}}} = 0.991$. (b) Makhlin invariants G_1 , G_2 , and G_3 , as functions of the inter-qubit coupling J_e . Other parameters are $L = 4$, $\Delta B_1 = 18 \text{ MHz}$, $\Delta B_2 = 7 \text{ MHz}$, $T_e = 1.4 \mu\text{s}$, $T_S = 2 \text{ ns}$, $J_S = \pi/T_S$, $T_g = 1 \mu\text{s}$.

qubit are assumed to have the same field value). In this figure, the axes give the nominal field gradients that are assumed in order to determine the pulse sequences that execute the necessary z rotations. The actual magnetic fields used in the calculation are modified, however, by the addition of Gaussian random field noise with standard deviation $\sigma_B = 1 \text{ MHz}$. The difference between the nominal and actual field values leads to errors in the single-qubit rotations of Eq. (14). As the Makhlin invariants are unaffected by single-qubit rotations, the results are essentially the same as for $\sigma_B = 0$ (not shown). Nevertheless, we find that large values ($\sim 100 \text{ MHz}$) of the field gradients lead to sizable departures from the ideal CZ gate, due to errors in the SWAP gates induced by the gradients. But for $\Delta B_1, \Delta B_2 < 50 \text{ MHz}$, the Makhlin

invariants remain close to the ideal ones. Use of composite pulse shaping is expected to allow for successful operation in the larger gradient regime as well.

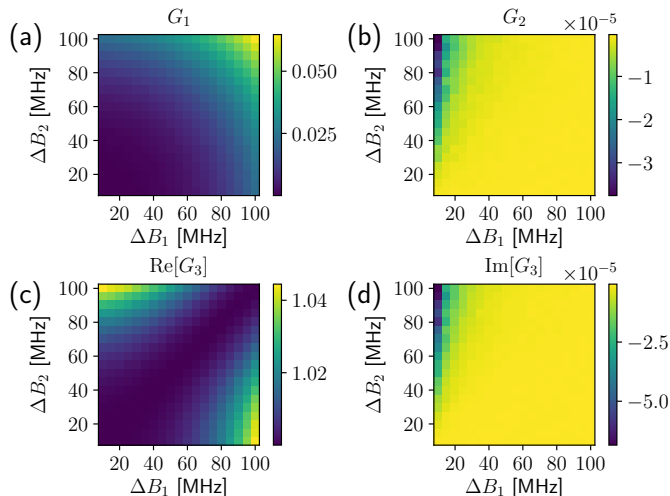


FIG. 10. Makhlin invariants G_1 , G_2 , and G_3 as functions of the nominal magnetic field gradients across each qubit. The true magnetic field for each data point is modified by the addition of Gaussian random field noise with standard deviation $\sigma_B = 1$ MHz. Other parameters are $L = 4$, $J_e = \pi/(2T_e)$, $T_e = 1.4 \mu s$, $n_T = 2$, $T_S = 2$ ns, $J_S = \pi/T_S$, $T_g = 1 \mu s$. Results are averaged over 40 disorder realizations.

Unlike the Makhlin invariants, the CZ gate probabilities are reduced by inaccurate z rotations, and thus by differences between the nominal and actual magnetic field gradients in the system. Fig. 11 shows the return probabilities in the presence of $\sigma_B = 1$ MHz Gaussian field noise when the nominal gradients are $\Delta B_1 = 18$ MHz and $\Delta B_2 = 7$ MHz. We find that the mean return probability is lowered from 0.991 in the noiseless case to 0.968 in the presence of noise. This suggests that reliable knowledge of the field gradients is crucial for obtaining accurate ST qubit gates.

An alternative metric for the quality of the physical CZ gate is given by the fidelity:^{42,43}

$$f = \frac{1}{20} (\text{Tr}[U_{CZ,p} U_{CZ,p}^\dagger] + |\text{Tr}[U_{CZ,p}^\dagger CZ^*]|^2), \quad (17)$$

where $CZ^* = U_4 U_3 CZ U_2 U_1$ is the generalized CZ consisting of the ordinary CZ preceded by arbitrary one-qubit unitaries $U_{1,2}$ of the two qubits, and followed by the arbitrary unitaries $U_{3,4}$. Furthermore, $U_{CZ,p}$ is the DTC part ($[U_{SWAP}(T_S) U_{evo}(T_e)]^2$) of the physical CZ gate projected down to the computational subspace, and CZ^* is optimized over the parameters $\alpha_i, \beta_i, \gamma_i, \delta_i$ defining the one-qubit unitaries $U_i = e^{i\alpha_i} \mathcal{R}_z(\beta_i) \mathcal{R}_y(\gamma_i) \mathcal{R}_z(\delta_i)$. With this definition, the optimized fidelity of the physical CZ gate is shown as a function of the magnetic field gradients in Fig. 12. For gradients below 50 MHz, the optimized fidelity reaches values in excess of 0.995, indicating that single-qubit rotations are the limiting factor in achieving

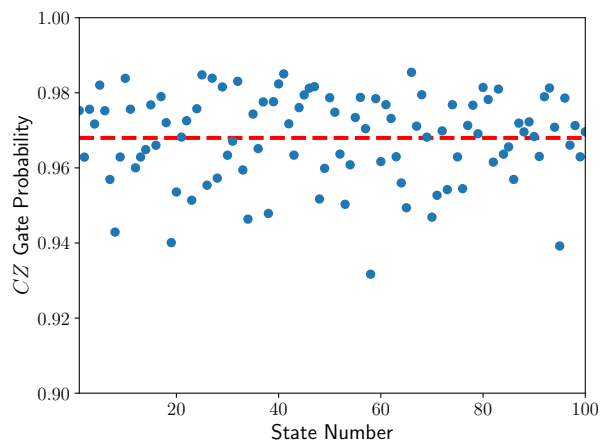


FIG. 11. CZ gate probabilities for random initial product states of the ST qubits, for which the true magnetic field for each data point is modified by the addition of Gaussian random field noise with standard deviation $\sigma_B = 1$ MHz. The red dashed line shows the mean value $\overline{p_{CZ}} = 0.968$. Other parameters are $L = 4$, $\Delta B_1 = 18$ MHz, $\Delta B_2 = 7$ MHz, $J_e = \pi/(2T_e)$, $T_e = 1.4 \mu s$, $n_T = 2$, $T_S = 2$ ns, $J_S = \pi/T_S$, $T_g = 1 \mu s$. Results are averaged over 20 disorder realizations.

an accurate gate in this case. While z rotations can be performed by turning off the intra-qubit exchange coupling J_S for the appropriate length of time, thereby allowing the system to evolve in the “always on” field gradients, perfect x rotations cannot be similarly achieved by applying a single value of J_S for a given time, as the axis of rotation is tilted due to the gradients. This again highlights the need for pulse shaping methods to improve single-qubit rotations.

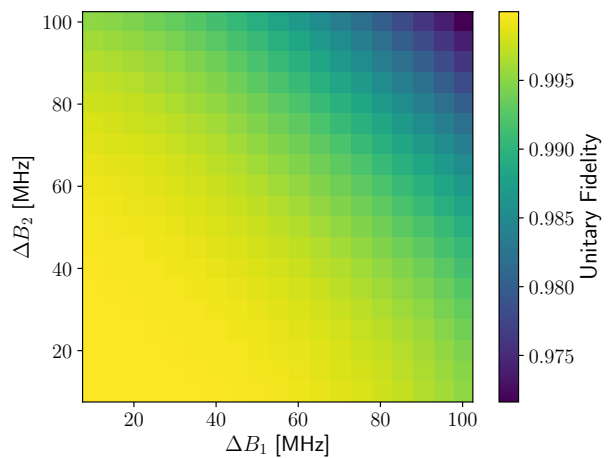


FIG. 12. Optimized unitary fidelity of Eq. (17) as a function of the magnetic field gradients across each qubit. Other parameters are $L = 4$, $J_e = \pi/(2T_e)$, $T_e = 1.4 \mu s$, $n_T = 2$, $T_S = 2$ ns, $J_S = \pi/T_S$, $T_g = 1 \mu s$.

Thus far we have considered a two-qubit CZ gate that requires two periods of the SWAP DTC driving protocol, with a modified value of J_e that maximizes the gate performance instead of preserving the initial state. It is natural to ask whether a CZ gate could also be executed using a single period of inter-qubit evolution. That is indeed the case, as illustrated in Fig. 13(a), which shows that for a single evolution period such that $J_e T_e = \pi$, the Makhlin invariants are close to their ideal values. Here, the evolution is not followed by the subsequent intra-qubit SWAP pulses of the DTC protocol, as these amount to unnecessary additional single-qubit rotations. However, the corresponding CZ gate probabilities for the optimal value of J_e are very poor [Fig. 13(a)]. This is due to the fact that the one-period protocol lacks the spin-echo behavior of the two-period version discussed above, which cancels the continuous z rotations of ST qubits with finite field gradients. Nevertheless, one can still achieve high CZ gate probabilities by selectively rotating each qubit through different angles $\theta_{z,1}, \theta_{z,2}$, such that the total rotation for each qubit at the end of the gate is the required $\mathcal{R}_{z,\pi/2}$. This is seen in Fig. 14, which displays the CZ gate probability as a function of single-qubit rotation angles applied to each qubit after the inter-qubit evolution part of the gate. The optimal choices of rotation angles depend on the field gradients across each qubit; in Fig. 14 the highest return probability attained is 0.980, comparable to that of the two-period CZ protocol.

The advantage of the one-period protocol (apart from the two-fold reduction in gate time) can be seen by considering the Makhlin invariants as functions of the magnetic field gradients [Fig. 15]. The invariants remain within 10^{-5} of their ideal values throughout the range considered, thus showing considerable improvement from the two-period case at large gradients. This suggests that optimizing over arbitrary single-qubit operations before and after an ideal CZ gate, in the manner of Eq. (17), should lead to very high fidelities. We confirm this expectation, as shown in Fig. 16, where the lowest infidelity over the range of gradients considered is only $\sim 5 \times 10^{-7}$. Infidelities obtained in experiments will likely be higher due to single-qubit rotation errors. Despite the significantly improved fidelities of the one-period protocol over the two-period version, the fact that the required z rotations are gradient-dependent may present further experimental challenges. This would necessitate adaptive control of the pulse sequence, in response to a prior measured value of the field gradient. The two-period sequence, on the other hand, always involves z rotations of $\pi/2$ for each qubit, regardless of the gradient strength, such that the pulse sequence does not need to be changed “on the fly.”

VIII. CONCLUSIONS

We have shown that driving exchange interactions, as opposed to performing single-spin rotations, in QD

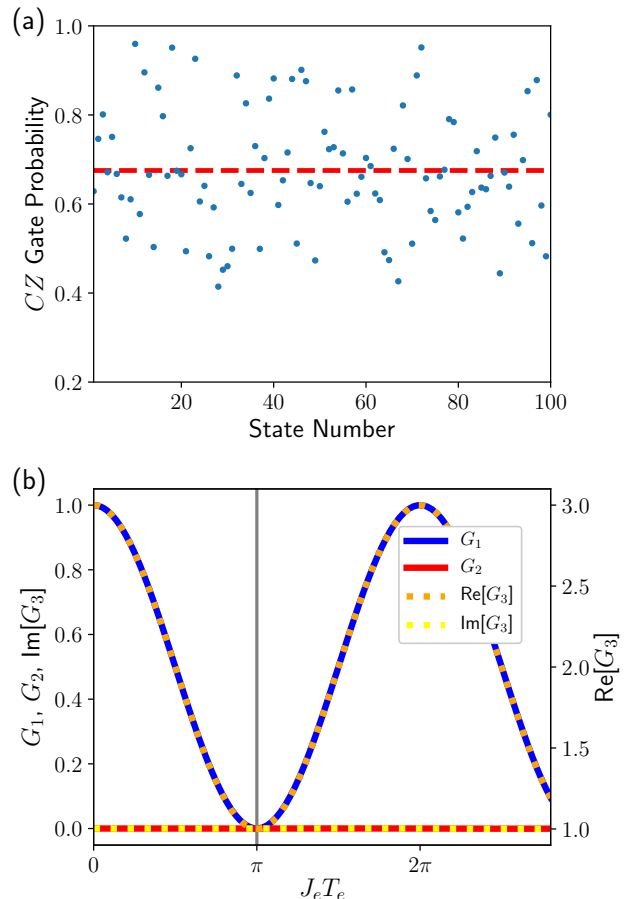


FIG. 13. (a) CZ gate probability for the $n_T = 1$ protocol, using the optimal $J_e = \pi/T_e$, indicated by the vertical gray line in panel (b). The red dashed line indicates the mean CZ gate probability $\overline{p_{CZ}} = 0.675$. (b) Makhlin invariants for the $n_T = 1$ protocol for the CZ gate. Other parameters are $L = 4$, $\Delta B_1 = 18$ MHz, $\Delta B_2 = 7$ MHz, $\sigma_B = 0$, $T_e = 1.4$ μ s, $T_g = 1$ μ s.

spin chains leads to an alternative route to time crystal physics that can be used for the preservation and manipulation of quantum states. We demonstrated that such driving is particularly useful for preserving the entangled singlet and triplet spin states often used as logical qubit states for quantum computation, and on average preserves arbitrary states on the Bloch sphere better than the undriven case. In addition, we uncovered additional signatures of the exchange-driven time crystal phase, including a $4T$ periodicity of the singlet return probability that runs counter to the $2T$ periodicity normally encountered in such systems. We also considered applications of this time crystal physics to the design of exchange-driven quantum gates for singlet-triplet qubits. In particular, we showed that a simple modification of the SWAP-DTC protocol yields a high-fidelity CZ gate, up to single-qubit operations. These results suggest that time crystal physics may be beneficial to quantum information applications based on QD spin qubits.

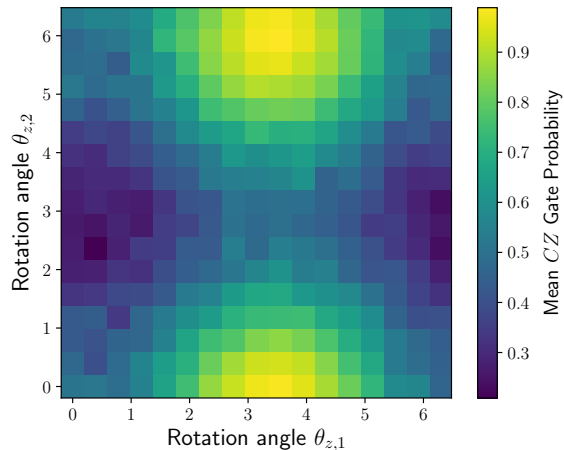


FIG. 14. Mean CZ gate probability for the $n_T = 1$ protocol, varying the single-qubit rotation angles applied after the two-qubit evolution. Other parameters are $L = 4$, $\Delta B_1 = 18$ MHz, $\Delta B_2 = 7$ MHz, $\sigma_B = 0$, $J_e = \pi/T_e$, $T_e = 1.4 \mu\text{s}$, $T_g = 1 \mu\text{s}$. Results are averaged over 100 randomly selected initial states, which are product states of generic ST qubit states.

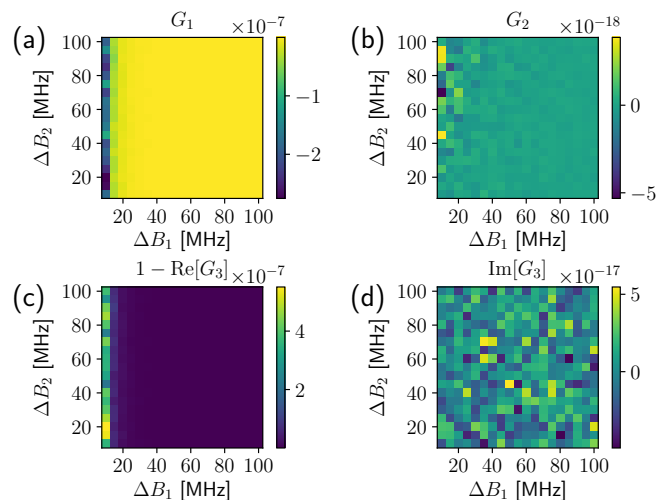


FIG. 15. Makhlin invariants G_1 , G_2 , and G_3 as functions of the nominal magnetic field gradients across each qubit. (Note that $1 - \text{Re}[G_3]$ is plotted in (c)). The true magnetic field for each data point is modified by the addition of Gaussian random field noise with standard deviation $\sigma_B = 1$ MHz. Other parameters are $L = 4$, $J_e = \pi/T_e$, $T_e = 1.4 \mu\text{s}$, $n_T = 1$, $T_g = 1 \mu\text{s}$. Results are averaged over 40 disorder realizations.

ACKNOWLEDGMENTS

We thank Bikun Li and Fernando Calderon-Vargas for helpful discussions. This work is supported by DARPA Grant No. D18AC00025.

- ¹ R. Augusiak, F. M. Cucchietti, and M. Lewenstein, Many-Body Physics from a Quantum Information Perspective, in *Modern Theories of Many-Particle Systems in Condensed Matter Physics*, Vol. 843, edited by D. C. Cabra, A. Honecker, and P. Pujol (Springer Berlin Heidelberg, Berlin, Heidelberg, 2012) pp. 245–294.
- ² B. Zeng, X. Chen, D.-L. Zhou, and X.-G. Wen, *Quantum Information Meets Quantum Matter: From Quantum Entanglement to Topological Phases of Many-Body Systems*, Quantum Science and Technology (Springer New York, New York, NY, 2019).
- ³ J. Preskill, Quantum Computing in the NISQ era and beyond, *Quantum* **2**, 79 (2018).
- ⁴ J. R. McClean, J. Romero, R. Babbush, and A. Aspuru-Guzik, The theory of variational hybrid quantum-classical algorithms, *New Journal of Physics* **18**, 023023 (2016).
- ⁵ A. Kandala, A. Mezzacapo, K. Temme, M. Takita, M. Brink, J. M. Chow, and J. M. Gambetta, Hardware-efficient variational quantum eigensolver for small molecules and quantum magnets, *Nature* **549**, 242 (2017).
- ⁶ D. V. Else, B. Bauer, and C. Nayak, Floquet Time Crystals, *Physical Review Letters* **117**, 090402 (2016).

- ⁷ N. Yao, A. Potter, I.-D. Potirniche, and A. Vishwanath, Discrete Time Crystals: Rigidity, Criticality, and Realizations, *Physical Review Letters* **118**, 030401 (2017).
- ⁸ D. A. Abanin, E. Altman, I. Bloch, and M. Serbyn, Colloquium: Many-body localization, thermalization, and entanglement, *Reviews of Modern Physics* **91**, 021001 (2019).
- ⁹ D. V. Else, C. Monroe, C. Nayak, and N. Y. Yao, Discrete Time Crystals, *Annual Review of Condensed Matter Physics* **11**, 467 (2020).
- ¹⁰ V. Khemani, M. Hermele, and R. Nandkishore, Localization from Hilbert space shattering: From theory to physical realizations, *Physical Review B* **101**, 174204 (2020).
- ¹¹ V. Khemani, R. Moessner, and S. L. Sondhi, A Brief History of Time Crystals, *arXiv.org* (2019).
- ¹² N. Y. Yao, C. R. Laumann, and A. Vishwanath, Many-body localization protected quantum state transfer, *arXiv.org* (2015).
- ¹³ R. A. Santos, F. Iemini, A. Kamenev, and Y. Gefen, Multidimensional dark space and its underlying symmetries: towards dissipation-protected qubits, *arXiv:2002.00237* (2020).
- ¹⁴ J. Zhang, P. W. Hess, A. Kyprianidis, P. Becker, A. Lee, J. Smith, G. Pagano, I.-D. Potirniche, A. C. Potter, A. Vishwanath, N. Y. Yao, and C. Monroe, Observation

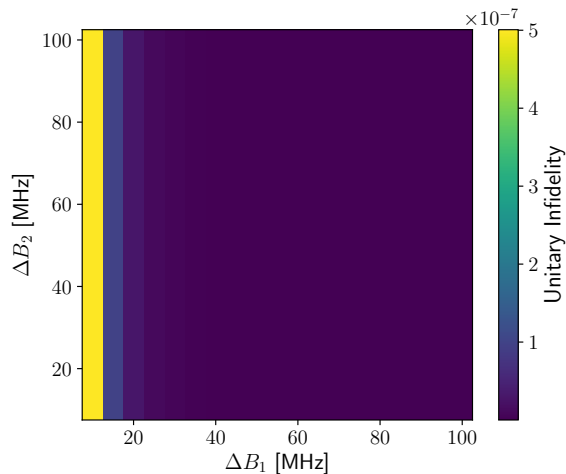


FIG. 16. CZ gate infidelity for the one-period protocol ($n_T = 1$) as a function of the magnetic field gradients across each qubit. The infidelity at each point is optimized over single-qubit gate parameters. Other parameters are $L = 4$, $J_e = \pi/T_e$, $T_e = 1.4 \mu\text{s}$, $T_g = 1 \mu\text{s}$.

of a discrete time crystal, *Nature* **543**, 217 (2017).

¹⁵ S. Choi, J. Choi, R. Landig, G. Kucsko, H. Zhou, J. Isoya, F. Jelezko, S. Onoda, H. Sumiya, V. Khemani, C. von Keyserlingk, N. Y. Yao, E. Demler, and M. D. Lukin, Observation of discrete time-crystalline order in a disordered dipolar many-body system, *Nature* **543**, 221 (2017).

¹⁶ M. Pioro-Ladrière, T. Obata, Y. Tokura, Y. S. Shin, T. Kubo, K. Yoshida, T. Taniyama, and S. Tarucha, Electrically driven single-electron spin resonance in a slanting zeeman field, *Nature Physics* **4**, 776 (2008).

¹⁷ T. F. Watson, S. G. J. Philips, E. Kawakami, D. R. Ward, P. Scarlino, M. Veldhorst, D. E. Savage, M. G. Lagally, M. Friesen, S. N. Coppersmith, M. A. Eriksson, and L. M. K. Vandersypen, A programmable two-qubit quantum processor in silicon, *Nature* **555**, 633 (2018).

¹⁸ A. J. Sigillito, J. C. Loy, D. M. Zajac, M. J. Gullans, L. F. Edge, and J. R. Petta, Site-Selective Quantum Control in an Isotopically Enriched $^{28}\text{Si}/\text{Si}_{0.7}\text{Ge}_{0.3}$ Quadruple Quantum Dot, *Physical Review Applied* **11**, 061006 (2019).

¹⁹ K. Takeda, A. Noiri, J. Yoneda, T. Nakajima, and S. Tarucha, Resonantly Driven Singlet-Triplet Spin Qubit in Silicon, *Physical Review Letters* **124**, 117701 (2020).

²⁰ J. R. Petta, A. C. Johnson, J. M. Taylor, E. A. Laird, A. Yacoby, M. D. Lukin, C. M. Marcus, M. P. Hanson, and A. C. Gossard, Coherent Manipulation of Coupled Electron Spins in Semiconductor Quantum Dots, *Science* **309**, 2180 (2005).

²¹ M. D. Reed, B. M. Maune, R. W. Andrews, M. G. Borselli, K. Eng, M. P. Jura, A. A. Kiselev, T. D. Ladd, S. T. Merkel, I. Milosavljevic, E. J. Pritchett, M. T. Rakher, R. S. Ross, A. E. Schmitz, A. Smith, J. A. Wright, M. F. Gyure, and A. T. Hunter, Reduced Sensitivity to Charge Noise in Semiconductor Spin Qubits via Symmetric Operation, *Physical Review Letters* **116**, 110402 (2016).

²² F. Martins, F. K. Malinowski, P. D. Nissen, E. Barnes, S. Fallahi, G. C. Gardner, M. J. Manfra, C. M. Marcus, and F. Kuemmeth, Noise Suppression Using Symmetric

Exchange Gates in Spin Qubits, *Physical Review Letters* **116**, 116801 (2016).

²³ H. Qiao, Y. P. Kandel, J. S. Van Dyke, S. Fallahi, G. C. Gardner, M. J. Manfra, E. Barnes, and J. M. Nichol, Floquet-Enhanced Spin Swaps, arXiv.org (2020).

²⁴ J. Levy, Universal Quantum Computation with Spin-1/2 Pairs and Heisenberg Exchange, *Physical Review Letters* **89**, 147902 (2002).

²⁵ M. D. Shulman, O. E. Dial, S. P. Harvey, H. Bluhm, V. Umansky, and A. Yacoby, Demonstration of Entanglement of Electrostatically Coupled Singlet-Triplet Qubits, *Science* **336**, 202 (2012).

²⁶ X. Wang, L. S. Bishop, J. P. Kestner, E. Barnes, K. Sun, and S. D. Sarma, Composite pulses for robust universal control of singlet-triplet qubits, *Nature Communications* **3**, 1 (2012).

²⁷ F. A. Calderon-Vargas and J. P. Kestner, Directly accessible entangling gates for capacitively coupled singlet-triplet qubits, *Physical Review B* **91**, 035301 (2015).

²⁸ J. M. Nichol, L. A. Orona, S. P. Harvey, S. Fallahi, G. C. Gardner, M. J. Manfra, and A. Yacoby, High-fidelity entangling gate for double-quantum-dot spin qubits, *npj Quantum Information* **3**, 1 (2017).

²⁹ D. Buterakos, R. E. Throckmorton, and S. D. Sarma, Simulation of the coupling strength of capacitively coupled singlet-triplet qubits, *Physical Review B* **100**, 075411 (2019).

³⁰ R. K. L. Colmenar and J. P. Kestner, Stroboscopically robust gates for capacitively coupled singlet-triplet qubits, *Physical Review A* **99**, 012347 (2019).

³¹ P. Cerfontaine, R. Otten, M. A. Wolfe, P. Bethke, and H. Bluhm, High-fidelity gate set for exchange-coupled singlet-triplet qubits, *Physical Review B* **101**, 155311 (2020).

³² E. Barnes, J. M. Nichol, and S. E. Economou, Stabilization and manipulation of multispin states in quantum-dot time crystals with Heisenberg interactions, *Physical Review B* **99**, 035311 (2019).

³³ B. Li, J. S. V. Dyke, A. Warren, S. E. Economou, and E. Barnes, Discrete time crystal in the gradient-field Heisenberg model, *Physical Review B* **101**, 115303 (2020).

³⁴ P. Weinberg and M. Bukov, QuSpin: a Python package for dynamics and exact diagonalisation of quantum many body systems part I: spin chains, *SciPost Physics* **2**, 003 (2017).

³⁵ E. Barnes, D.-L. Deng, R. E. Throckmorton, Y.-L. Wu, and S. Das Sarma, Noise-induced collective quantum state preservation in spin qubit arrays, *Physical Review B* **93**, 085420 (2016).

³⁶ M. P. Wardrop and A. C. Doherty, Exchange-based two-qubit gate for singlet-triplet qubits, *Physical Review B* **90**, 045418 (2014).

³⁷ J. A. Jones, NMR quantum computation, *Progress in Nuclear Magnetic Resonance Spectroscopy* **38**, 325 (2001).

³⁸ E. Barnes, X. Wang, and S. D. Sarma, Robust quantum control using smooth pulses and topological winding, *Scientific Reports* **5**, 1 (2015).

³⁹ J. Zeng, C. H. Yang, A. S. Dzurak, and E. Barnes, Geometric formalism for constructing arbitrary single-qubit dynamically corrected gates, *Physical Review A* **99**, 052321 (2019).

⁴⁰ Y. Makhlin, Nonlocal Properties of Two-Qubit Gates and Mixed States, and the Optimization of Quantum Computations, *Quantum Information Processing* **1**, 243 (2002).

- ⁴¹ J. Zhang, J. Vala, S. Sastry, and K. B. Whaley, Geometric theory of nonlocal two-qubit operations, *Physical Review A* **67**, 042313 (2003).
- ⁴² H. P. Pedersen, N. M. Møller, and K. Mølmer, Fidelity of quantum operations, *Physics Letters A* **367**, 47 (2007).
- ⁴³ S. E. Economou and E. Barnes, Analytical approach to swift nonleaky entangling gates in superconducting qubits, *Physical Review B* **91**, 161405 (2015).